Dissociative recombination of HF^+

J. B. Roos,[1] Å. Larson,[1,*] and A. E. Orel[2]
[1]*Department of Physics, Stockholm University, AlbaNova University Center, S-106 91 Stockholm, Sweden*
[2]*Department of Applied Science, University of California, Davis, Davis, California 95616, USA*
(Received 29 May 2008; published 12 August 2008)

The direct mechanism of dissociative recombination of HF^+ is studied using both time-dependent and time-independent methods, where the dynamics on 30 resonant states is explored. The relevant electronic states are calculated *ab initio* by combining electron scattering calculations with multireference configuration interaction structure calculations. For collision energies between 0.04 and 10 eV, we obtain qualitative agreement with experiment. At 1.9 eV there is a sharp threshold in both the experimental and theoretical cross sections that can be explained by the opening of new asymptotic limits. The measured cross section below 0.04 eV is not reproduced due to the neglect of the electronic couplings between the neutral states. We examine the validity of the local approximation for treating autoionization from the resonant states included in this study.

DOI: 10.1103/PhysRevA.78.022508 PACS number(s): 31.50.Df, 34.80.Lx, 31.15.xv, 34.80.Ht

I. INTRODUCTION

The interactions of electrons and photons with hydrogen fluoride is of importance in the modeling of chemical lasers involving HF as well as rare-gas fluoride lasers. More recently, HF and HF^+ have become of interest in the semiconductor industry due to the presence of these molecules in etching plasmas [1]. The cross sections for such processes involving HF and HF^+ are critical in understanding the chemistry of these plasmas. In addition, the HF molecule occurs in nature and is one of a number of molecules that has been observed in interstellar clouds [2]. It has also been found in the planetary atmosphere of Venus [3]. As the simplest hydrogen halide, HF and HF^+ have served as benchmarks for theoretical studies. The potential curves for HF and HF^+ have been calculated using a number of *ab initio* methods [4–9].

We have carried out theoretical calculations on dissociative recombination (DR) of HF^+. Dissociative recombination is the key process in the physics of plasmas where molecular ions are present. In DR, the electron is resonantly captured by the ion, losing its energy either to electronic or to rovibronic excitation of the resulting neutral molecule. In the first case, the so-called "direct process" [10] of DR, the electron is captured into an excited state of the neutral molecule. The molecule will then stabilize through dissociation. In the second process a rovibronically excited Rydberg state converging to the ground state of the ion is formed. This decays either by a direct dissociation or predissociation through couplings to electronic states that are open for dissociation [11].

In the ion-storage ring CRYRING, the cross section for DR of HF^+ has been measured [12] for collision energies between 0.0001 and 2 eV. The cross section of this ion is smaller than for other diatomic molecules with a thermal rate coefficient of 1.96×10^{-8} cm^3 s^{-1} at 300 K. In this experiment, the cross section for the formation of the ion pair $H^+ + F^-$ was also determined. It was found to be relatively large, about 14% of the DR cross section at a collision energy of 0.02 eV. Both cross sections show interesting structures that were attributed to competition between the direct and indirect processes [12]. Similar structures have previously been seen in photo ion-pair experiments, where the dissociation into the ion pair $H^+ + F^-$ is studied using photoexcitation of the ground state $X\,^2\Sigma^+$ HF molecule into one of the bound Rydberg states of HF [13–15].

In this study, we will only include the direct process of DR. When the electron is captured into the resonant state, the molecule can either autoionize (reemit the electron) or dissociate. When the potential energy curve of the neutral state has crossed the ionic ground state potential, autoionization is no longer possible and the resonant state becomes an electronically bound state. The cross section presented here corresponds to the total cross section for dissociation in electron recombination with HF^+, i.e., the sum of the cross section for DR and ion-pair formation.

Section II describes how the relevant diabatic electronic states are determined by combining electron scattering calculations with extensive multireference configuration interaction calculations. The details of the dynamics calculations are contained in Sec. III, where we describe both the time-dependent and time-independent methods that are used to study the reaction. Using the time-independent method, we explore the validity of the so-called local approximation for treating autoionization. This approximation may fail if the resonant state is crossing the ion potential close to its minimum and hence it must be considered that autoionization is not possible into the complete set of vibrational eigenstates of the ion. Finally, in Sec. IV the results are presented and the role of the direct vs indirect processes is discussed. Unless otherwise stated, atomic units are used throughout the paper.

II. POTENTIAL ENERGY CURVES

A. Scattering calculations

We determine the relevant electronic state potentials in all symmetries. The resonance energy and the autoionization width are obtained from electron scattering calculations. In

*Corresponding author; aasal@physto.se

this set of calculations, the complex Kohn variational method is used as described in [16]. In this method, the electronic trial wave function of the $(N+1)$-electron scattering system is expanded as

$$\Psi = \sum_{\Gamma} A[\Phi_{\Gamma}(\mathbf{x}_1, \ldots, \mathbf{x}_N) F_{\Gamma}(\mathbf{x}_{N+1})] + \sum_{\mu} d_{\mu} \Theta_{\mu}(\mathbf{x}_1, \ldots, \mathbf{x}_{N+1}). \tag{1}$$

The first sum is denoted as the P-space portion of the wave function and runs over the energetically open target states, where Φ_{Γ} are the N-electron target eigenstates, $\mathbf{x}_i$ denotes space-spin coordinates, and A antisymmetrizes the coordinates of the target and scattered electrons. In the second sum, the Θ_{μ} are square-integrable $N+1$ configuration state functions (CSFs), which are used to describe short-range correlations and the effects of closed channels. These functions also contain information about the resonance portion of the scattering wave function. This sum is denoted as the Q-space portion of the wave function. In the case of HF^+, the ground state of the system is $^2\Pi$ and there is a low-lying $^2\Sigma$ excited state. Therefore, three channels (the two degenerate components of the Π state and the Σ state) were treated in the P space. However, at low scattering energies only the two degenerate Π channels may be open.

There are two classes of terms included in the Q space. The first class of functions is the set of all $(N+1)$-electron CSFs that can be formed from the active space of target orbitals. These are terms which will relax any constraints implied by the strong orthogonality between the scattering functions F_{Γ} and the target orbitals. They are generally referred to as "penetration terms" [16]. We also include a second class of terms, "CI relaxation terms." These are all closed channels that can be formed from the set of target configurations used to build P space. These terms, combined with the penetration terms, constitute the correlation part of the trial wave function. For further information on this subject, we refer the reader to [16].

As the internuclear separation is increased, the resonant state becomes electronically bound and is determined through the use of standard quantum chemistry techniques, using a multireference configuration interaction (MRCI) calculation. To obtain the target state, a set of molecular orbitals were generated from a self-consistent-field calculation (SCF) using a contracted $(14s8p2d/11s7p2d)$ basis set for H and a $(10s7p2d/6s5p2d)$ triple-(ζ) basis set with polarization and additional functions to describe the negative ion for F. To obtain a more compact representation, a configuration interaction (CI) calculation on the neutral was carried out consisting of all singles and doubles, where the 1σ orbital is frozen and the active space is four orbitals, 2σ, 3σ, $1\pi_x$, and $1\pi_y$. The natural orbitals were abstracted from this calculation. The final target basis then consisted of eight natural orbitals with the highest occupation numbers, the lowest σ orbital which is frozen, three σ, and four π orbitals, two π_x and two π_y orbitals.

The electron scattering calculations are done for the $(N+1)$-electron system, meaning ten electrons are included. The target wave functions used in the calculation were obtained by freezing the first σ orbital and then carrying out a full CI in the smaller natural orbital space of seven orbitals in this $N+1$ system. This forms the first class of terms in the Q space mentioned above. The variational calculations included spherical harmonics up to $l=6$ and $|m|=4$. The calculations are carried out in each symmetry at a fixed internuclear distance. At the resonant energy E_{res}, the electron can be temporarily captured into a "metastable state," which will cause a sharp variation of the elastic scattering cross section. As the electron energy passes through the resonance energy E_{res}, the eigenphase sum will jump by π (see Fig. 1).

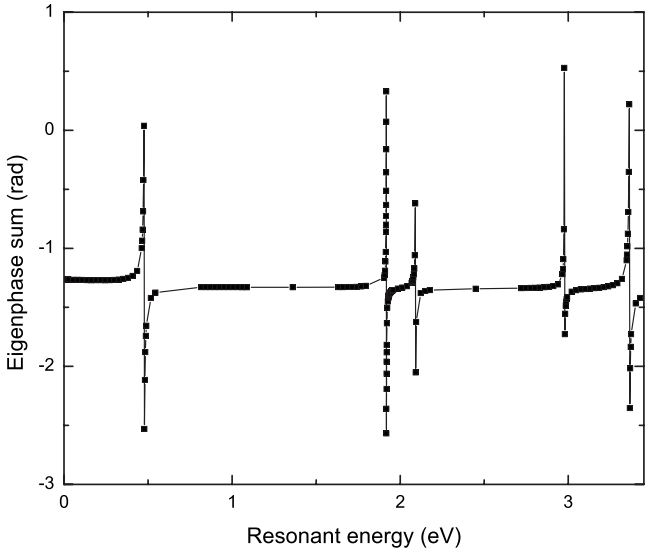

FIG. 1. The eigenphase sum from a scattering calculation of $^3\Pi$ symmetry at $R=1.9a_0$.

In order to determine the resonance energy $E_{res}(R)$ and autoionization width $\Gamma(R)$, we fit the eigenphase sum with a Breit-Wigner form [17]

$$\delta(E) = \delta_{res}(E) + \delta_{bg}(E) = \tan^{-1}\left(\frac{\Gamma}{2(E - E_{res})}\right) + a + bE + cE^2. \tag{2}$$

Here δ_{res} is the contribution to the eigenphase sum from the resonance and δ_{bg} is the background contribution. To obtain the potential energy curve of the resonant state, the ionic potential has to be added to the resonance energy $V(R) = V_{ion}(R) + E_{res}(R)$.

In the Franck-Condon region we find a total of 30 resonant states between the ionic ground state $X\ ^2\Pi$ and the first excited state of the ion $A\ ^2\Sigma^+$. There are nine $^1\Sigma^+$, nine $^3\Sigma^+$, five $^1\Pi$, five $^3\Pi$, one $^1\Delta$, and one $^3\Delta$ states.

B. Structure calculations

In order to determine the potential energy curves in the region where the resonant states become electronically bound we have carried out a set of MRCI calculations. To be able to merge the results of these calculations with the scattering calculation, the same basis set, natural orbitals, and MRCI used for the target wave function described above, must be used. This results in a CI of about 12 500 configu-

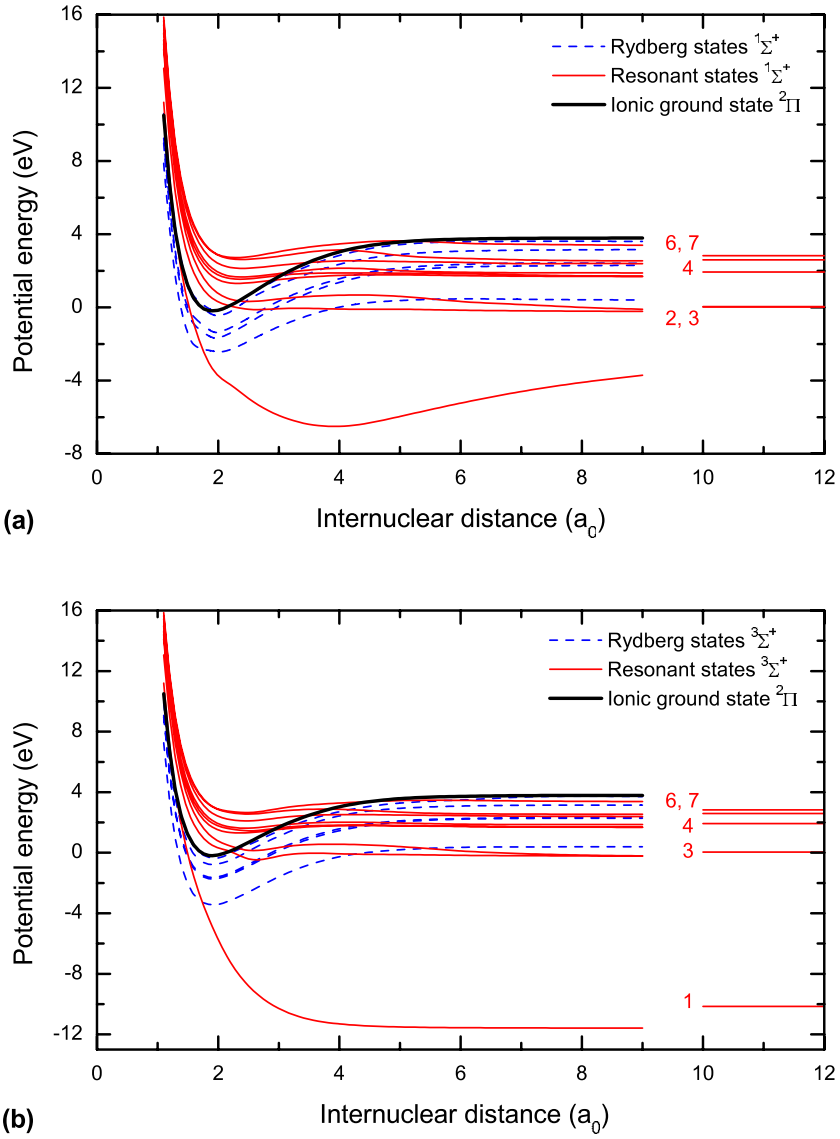

FIG. 2. (Color online) Diabatic states for HF of (a) $^1\Sigma^+$ and (b) $^3\Sigma^+$ symmetries. Also the ground state $X\,^2\Sigma^+$ of HF^+ is shown. The notation of the asymptotic energy limits for the resonant states follows the numbering in Table I.

rations. At each internuclear distance, for each spin coupling (singlet or triplet) and symmetry, 25 roots are obtained. Note that these roots can contain the doubly excited resonant states but also states that represent the background, that is, states that have the same character as the ground state of the ion $[(1\sigma)^2(2\sigma)^2(3\sigma)^2(1\pi)^3]$ plus an extra electron in a very diffuse orbital. By examining the CI coefficients these states are removed from the calculation. The calculations are carried out for internuclear distances in the range $1.1a_0 \leqslant R \leqslant 9.0a_0$, yielding adiabatic potential energy curves with energies both below and above the ground state of the HF^+ ion.

1. Diabatization

As mentioned above, both the ionization continuum and the Rydberg states converging to the ground state of the ion, will have dominant configurations corresponding to the configuration of the electronic ground state of the ion $[(1\sigma)^2(2\sigma)^2(3\sigma)^2(1\pi)^3]$ plus the extra electron in an outer orbital. The resonant states are Rydberg states converging to electronically excited ionic cores. These cores all have the (3σ) orbital singly excited. The resonant states are "diabatized" relative to the ionization continuum and the Rydberg states by tracking the states with dominant configurations where the (3σ) orbital is singly excited when the internuclear distance R is varied. The state associated with the ion-pair limit $H^+ + F^-$ at infinity has a configuration of $(1\sigma)^2(2\sigma)^2(3\sigma)^1(1\pi)^4(4\sigma)^1$. We find other resonant states with the same dominant configurations, but these are well separated in energy and the ion-pair state is for all distances lowest in energy.

The structure calculations do not show any avoided crossings between the resonant states in any of the symmetries. They are all well separated in energy so the diabatization is made by following the configuration of the excited ionic core toward larger internuclear distances assuming no crossing between the resonant states. Also it is assumed that there are no crossings among the Rydberg states.

The diabatic potential curves of the different symmetries are shown in Figs. 2–4. The potential energy curves of Σ^- symmetry are not displayed, since no resonant states of this symmetry exist.

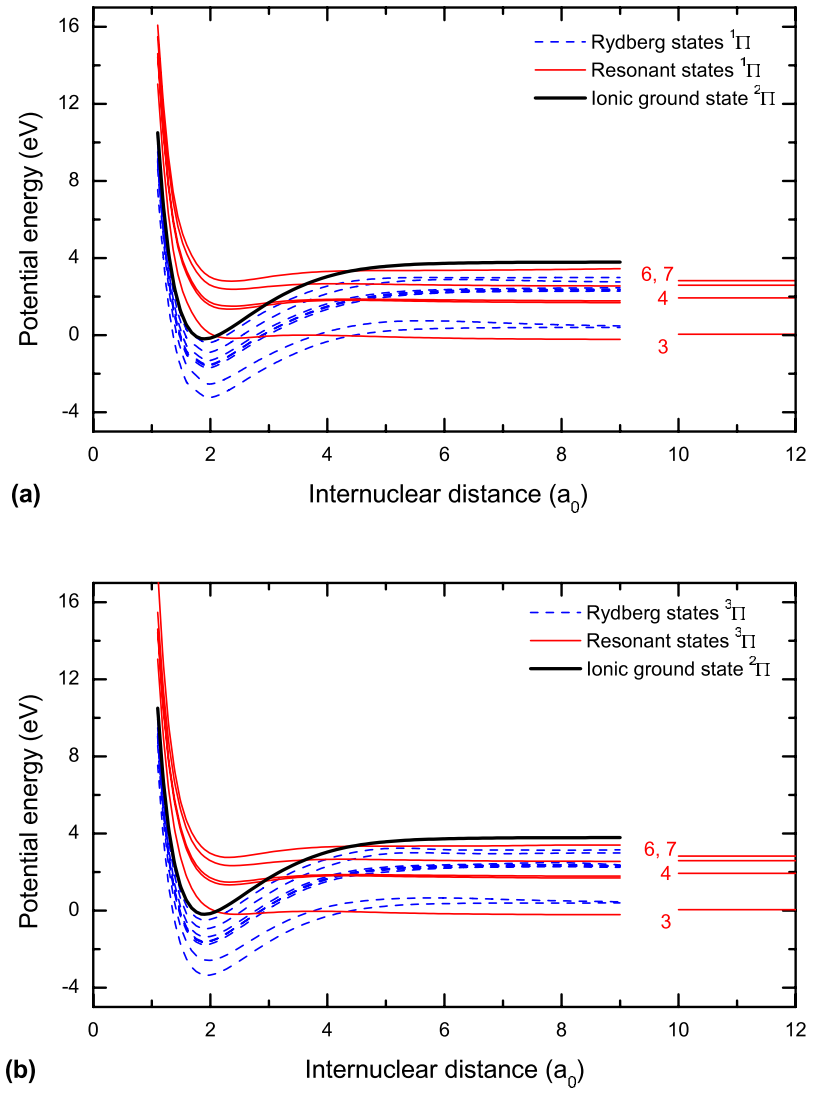

FIG. 3. (Color online) Diabatic states for HF of (a) $^1\Pi$ and (b) $^3\Pi$ symmetries.

2. Extrapolation

For the lower resonant states, electron scattering calculations are carried out in the region $1.1a_0 \leqslant R \leqslant 2.2a_0$ and for the higher states out to $R=3.0a_0$. As described above, the resonant state potentials determined using the scattering calculation are combined with the diabatic potentials extracted from the MRCI calculations. The MRCI calculations are carried out for $1.1a_0 \leqslant R \leqslant 9.0a_0$. In order to study the nuclear dynamics, we extrapolate the calculated potentials and autoionization widths to both smaller and larger internuclear distances.

It is important to have a good representation of the autoionization widths in the Franck-Condon region where the vibrational wave function of the ground vibrational state $v=0$ of the HF^+ ion is nonzero. This is the region where the electron will be captured. In Fig. 5, we show this vibrational wave function, calculated using a finite-difference method [18].

The amplitude of the vibrational wave function for the ground state of HF^+ at $R=1.1a_0$ is only 0.0004% of its maximal value. So the Franck-Condon overlap at smaller internuclear distances is negligible and the fit in this region we assume is not crucial. We then need the shape of the autoionization widths all the way to the crossing point of the resonant state with the ionic ground state after which autoionization is no longer possible. When the resonant states cross the ion, the autoionization widths smoothly go to zero. The autoionization widths for the lowest states are presented in Fig. 6.

It is necessary to determine the asymptotic limits of the potential energy curves. This is done by calculating the experimental energies of the asymptotic limits [19]. Since no spin-orbit couplings are included in the calculation of the potential energy curves and since the spin-orbit splitting is small for both the H and F atoms, we take the mean values of the energy levels with different J for the F atom and mean values for states with equal principal quantum number n for the H atom. We then apply the Wigner-Witmer rules [20] to examine how many states of the different symmetries are associated with each asymptotic limit. In Table I, we list the asymptotic limits of the diabatic resonant states included in the present study. The energy scale is relative to $v=0$ of the HF^+ ion.

The potentials dissociating into neutral fragments are assumed to have reached their asymptotic limit at $R=50.0a_0$.

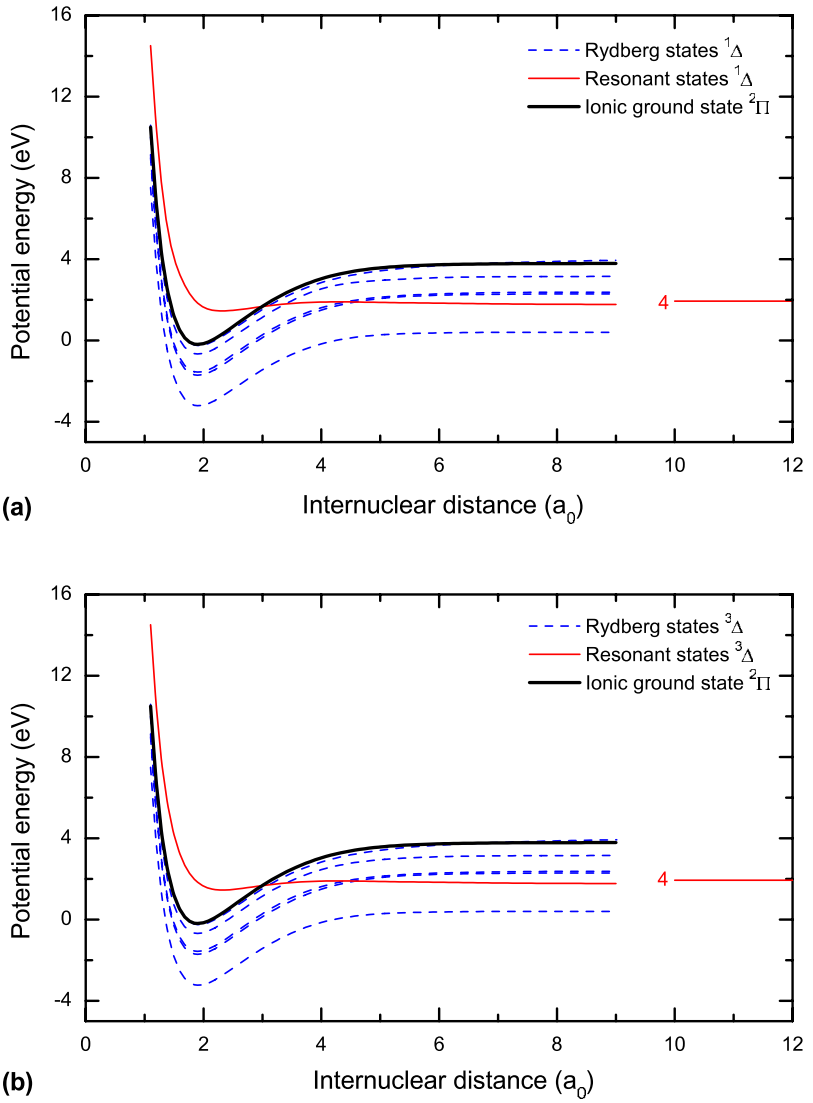

FIG. 4. (Color online) Diabatic states for HF of (a) $^1\Delta$ and (b) $^3\Delta$ symmetries.

The potential energy curve belonging to an ion-pair state is not flat in the asymptotic region due to the Coulomb attraction between the ion pair. Instead, the potential for such a state has the following form asymptotically:

$$V_1(R) = V_{final} - \frac{1}{R} - \frac{\alpha}{2R^4}, \tag{3}$$

where V_{final} is the asymptotic energy limit and $\alpha = 17.581 a_0^3$ is the polarizability of F^- [21]. We assume that the ion-pair state has this form at internuclear distances $R \geqslant 20a_0$ and interpolate between the calculated ion-pair state and the asymptotic form of the ion pair using spline interpolation. The calculated diabatic resonant potentials and autoionization widths are used for the dynamics calculations in order to determine the cross section for dissociative recombination.

III. REACTION DYNAMICS

The dissociative recombination process is now described using two different methods. First, we apply a time-dependent method, where wave packets are propagated along the resonant states. Autoionization is then included using a local model as described below. We have also calculated the cross section for the reaction, using a time-independent method, where it is numerically easier to include the nonlocal description of the autoionization from the resonant states.

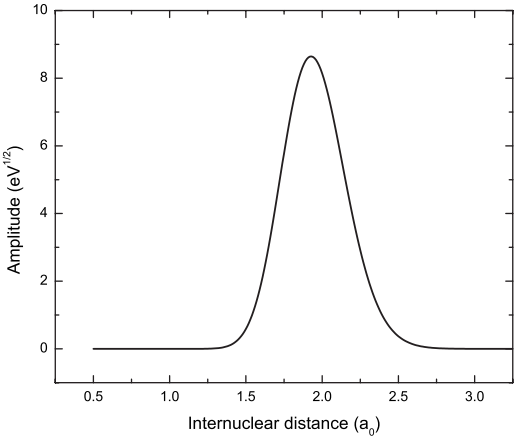

FIG. 5. The gound vibrational wave function of HF^+.

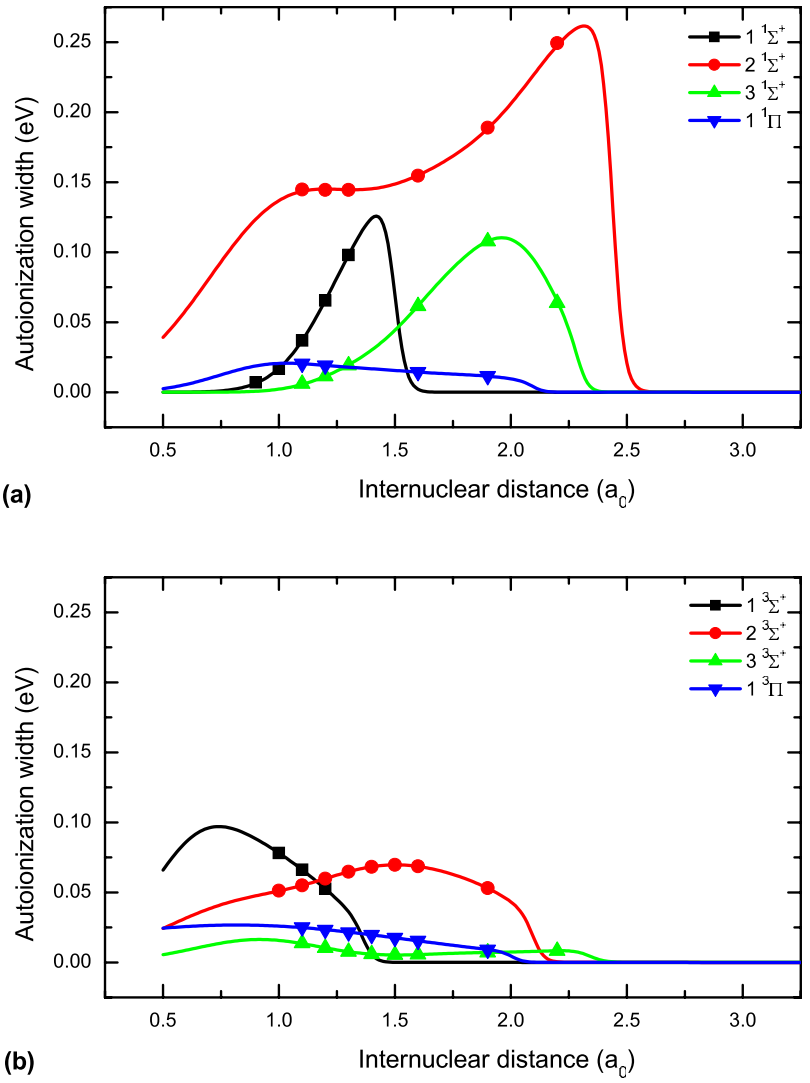

FIG. 6. (Color online) The autoionization widths for the four lowest (a) singlet and (b) triplet resonant states.

A. Time-dependent method

Using the time-dependent method, wave packets are propagated on the resonant states by solving the time-dependent Schrödinger equation

$$\imath\frac{\partial}{\partial t}\Psi_i(t,R) = \left(-\frac{1}{2\mu}\frac{\partial^2}{\partial R^2} + \tilde{V}_i(R)\right)\Psi_i(t,R), \tag{4}$$

with a Crank-Nicholson propagator [22]. Here μ is the reduced mass of HF.

The initial condition for the wave packets is given by [23]

$$\Psi_i(t=0,R) = \sqrt{\frac{\Gamma_i(R)}{2\pi}}\chi_{v_0}(R), \tag{5}$$

where χ_{v_0} is the vibrational wave function of the ground state of HF^+, calculated using a finite-difference method [18]. This vibrational wave function is shown in Fig. 5. Γ_i is the autoionization width of the resonant state i.

In the so-called local, Boomerang model [23], autoionization is included by letting the potentials be complex above the crossing point with the ionic ground state

$$\tilde{V}_i(R) = V_i(R) - \imath\frac{\Gamma_i(R)}{2}. \tag{6}$$

This approximation assumes that the total energy of the system is high enough that autoionization into a complete set of vibrational eigenstates is possible. When this approximation breaks down, i.e., for the lower resonant states, a nonlocal operator [24,25] to account for autoionization has to be used. This will be addressed in the following section.

In order to ensure the grid is fine enough to resolve the deBroglie wavelength of the dissociating fragments, we chose a small grid step of $dR=0.01a_0$. The initial wave function must be essentially zero at the end points of the grid. We therefore start our grid at $R_{min}=0.8a_0$ and as shown in Fig. 5, the vibrational wave function of the ground state of HF^+ is very close to zero at this value. The wave packets cannot be allowed to travel so far that they hit the edge of the grid. If that happens nonphysical reflections and interferences will occur. To ensure that the wave packets do not reach the end of the grid, we can chose a large grid ($R_{max}=80a_0$) and we add a complex absorbing potential [26,27] at large distances. This complex potential absorbs the outermost part of the

TABLE I. Asymptotic limits of the resonant states included in the present study. The energies are relative to the $v=0$ vibrational level of HF^+.

	Atomic states	Resonant states	Energy (eV)
1	$H(n=1)+F(^2P)$	$1\,^3\Sigma^+$	−10.1552
2	H^++F^-	$1\,^1\Sigma^+$	0.0170
3	$H(n=2)+F(^2P)$	$2\,^1\Sigma^+, 3\,^1\Sigma^+, 1\,^1\Pi,$ $2\,^3\Sigma^+, 3\,^3\Sigma^+, 1\,^3\Pi$	0.0437
4	$H(n=3)+F(^2P)$	$4\,^1\Sigma^+, 5\,^1\Sigma^+, 6\,^1\Sigma^+,$ $4\,^3\Sigma^+, 5\,^3\Sigma^+, 6\,^3\Sigma^+,$ $2\,^1\Pi, 3\,^1\Pi, 1\,^1\Delta,$ $2\,^3\Pi, 3\,^3\Pi, 1\,^3\Delta$	1.9323
5	$H(n=1)+F(^4P)$		2.5458
6	$H(n=4)+F(^4P)$	$7\,^1\Sigma^+, 8\,^1\Sigma^+, 4\,^1\Pi,$ $7\,^3\Sigma^+, 8\,^3\Sigma^+, 4\,^3\Pi$	2.5934
7	$H(n=1)+F(^2P)$	$9\,^1\Sigma^+, 5\,^1\Pi$ $9\,^3\Sigma^+, 5\,^3\Pi$	2.8249

wave packets before they hit the edge of the grid. The part of the wave packets that is absorbed corresponds to very high energy components that are not relevant for the reaction studied here. The wave packets must be propagated out to the asymptotic region, which in our case corresponds to $R \approx 10a_0$. The time that is needed to propagate the wave packets into this region will vary between the different resonant states and we use propagation times that vary between $t_{final}=300$ a.u. ≈ 7 fs to $t_{final}=1000$ a.u. ≈ 24 fs. The time step in the wave-packet propagation is $dt=0.1$ a.u. ≈ 0.002 fs. Convergence tests for the potentials were made where the time step, grid step, propagation time, and complex absorbing potential were varied until convergence was achieved.

When the wave packets have been propagated out in the asymptotic region, the partial cross sections are calculated by projecting the final wave packets onto energy-normalized eigenfunctions for the separated atoms $[\Phi_E^i(R)]$. This gives us the transition matrix element T_i,

$$T_i(E) = \lim_{t\to\infty} \langle \Phi_E^i(R) | \Psi_i(t,R) \rangle_R. \tag{7}$$

The cross section for state i is given by [23,28]

$$\sigma_i(E) = \frac{2\pi^3}{E} g |T_i(E)|^2, \tag{8}$$

where g is the multiplicity ratio of the neutral resonant state to the ionic state with the free electron. The total cross sec-

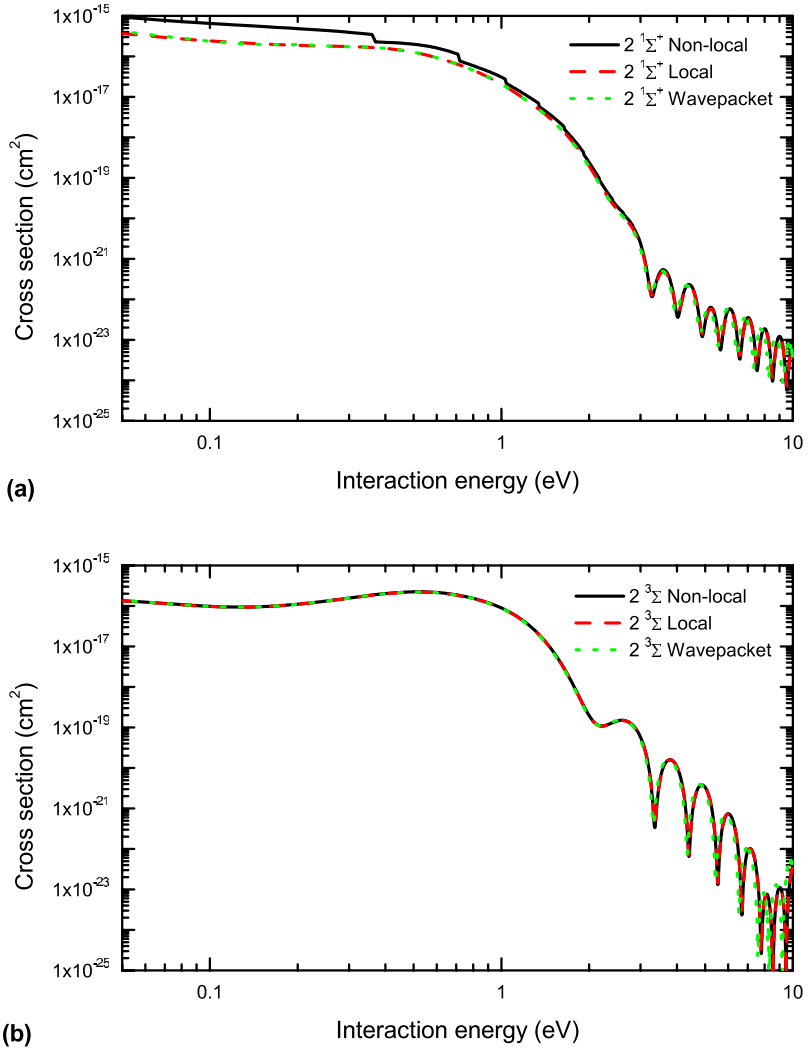

FIG. 7. (Color online) Contribution to the cross section from the (a) $2\,^1\Sigma^+$ and (b) $2\,^3\Sigma^+$ resonant states, calculated using the local, time-dependent (wave packet) method and the time-independent local, and nonlocal methods.

tion is given by the sum of the cross sections of the individual states

$$\sigma_{tot}(E) = \sum_i \sigma_i(E). \tag{9}$$

B. Time-independent method

We have also calculated the cross section for dissociative recombination of HF^+ using a time-independent method, where a nonlocal operator can be used to describe the autoioniation from the resonant states. As mentioned above, the nonlocal description of autoionization is necessary for the resonant states crossing the ion potential close to its minimum.

The time-independent description is based on a driven Schrödinger equation [29]

$$\left(E + \frac{1}{2\mu}\frac{\partial^2}{\partial R^2} - \hat{V}_i\right)\xi_i(R) = \sqrt{\frac{\Gamma_i(R)}{2\pi}}\chi_{v_0}(R), \tag{10}$$

where $\xi_i(R)$ is the nuclear wave function associated with the resonant state i. This is an inhomogeneous differential equation, where the "entry amplitude" is identical to the initial conditions for the wave packets [Eq. (5)] as described in the previous section. $\hat{V}_i$ is a nonlocal operator [24] for the complex resonant state energy. When this operator is acting on the wave function, we obtain

$$\hat{V}\xi_i(R) = V_i(R)\xi_i(R) - \imath\pi\sqrt{\frac{\Gamma_i(R)}{2\pi}} \times \sum_v \left\langle \chi_v(R') \middle| \sqrt{\frac{\Gamma_i(R')}{2\pi}} \middle| \xi_i(R') \right\rangle_{R'} \chi_v(R). \tag{11}$$

The summation goes over the energetically open vibrational states of the ion. Note that when the energy is high enough so closure for the vibrational states is obatined, the "local complex" resonant potential in Eq. (6) is obtained.

In order to solve the driven Schrödinger equation (10) numerically [30,31], a finite-element method is implemented using the discrete variable representation. To be able to calculate the dissociative wave function $\xi_{iv}(R)$ on a finite grid, we employ an exterior complex scaling [32,33], where the radial coordinate is rotated into the complex plane by the transformation

$$R \to \begin{cases} R, & R < R_0 \\ R_0 + (R - R_0)e^{\imath\theta}, & R \geqslant R_0. \end{cases} \tag{12}$$

In the expression above, the rotation is performed at a large internuclear distance ($R_0 = 10a_0$ in the present calculation). For a converged calculation, the radial wave function for $R < R_0$ will not depend on the scaling angle. Here, the scaling angle $\theta = 30°$ was used. The cross section for dissociative recombination [25] is given by the asymptotic wave function

$$\sigma_i(E) = \frac{\pi^2 K}{\mu E} g |\xi_{iv}(R_{0<})|^2, \tag{13}$$

where $R_{0<}$ is the last point before the radial grid becomes complex. In the expression above, $K = \sqrt{2\mu[E - V_i(R_{0<})]}$ is the wave number of the asymptotic fragments. The total cross section for dissociative recombination is obtained by summarizing the contributions from all resonant states. We have employed the time-independent method using both the nonlocal and local operators for treating autoionization from the resonant states.

IV. RESULTS AND DISCUSSION

A. Comparison between different models

As mentioned above, the cross section has been calculated using both the time-dependent and time-independent methods. Within the local approximation for describing autoionization out from the resonant states, the two methods should give the same resulting cross section and for all resonant states they do. Within the time-independent framework, we also explored the validity of the local approximation. By implementing the nonlocal operator, only autoionization into the energetically available vibrational levels of the HF^+ ion is considered. As mentioned above, the local approximation for treating autoionization may break down for resonant states that are crossing the ion potential close to its minimum. Also the difference between the local and nonlocal models is more significant if the magnitude of the autoionization width is larger and therefore the probability for autoionization is increased. In Fig. 7, we show the calculated cross section for the $2\,^1\Sigma^+$ [in (a)] and $2\,^3\Sigma^+$ [in (b)] resonant states using both the time-independent and time-dependent methods. As can be seen in Fig. 2, both these two resonant states have potential curves that are crossing the ion potential close to its minimum. However, if we compare the autoionization width (Fig. 6), we note that the width of the $2\,^1\Sigma^+$ state is larger than the width of the $2\,^3\Sigma^+$ resonant state.

For both resonant states, there is no difference between the calculated local time-independent and time-dependent cross sections. For the $2\,^1\Sigma^+$ resonant state, the nonlocal time-independent cross section is slightly larger at small energies and the thresholds effects from the opening of new vibrational states of HF^+ can be seen as sudden decreases in the cross section for dissociation. For the $2\,^3\Sigma^+$ resonant state with a smaller autoionization width, there is no observable difference between cross sections calculated using the nonlocal and local time-independent methods.

Using all three methods, the calculated cross section for the two resonant states show oscillations at larger energies. As will be seen below, similar oscillations are seen for all resonant states. These types of oscillations of a direct process have been seen before [34] and they can be understood by using a time-independent approach and analyze the energy dependence of the following matrix element:

$$P_{cap}(E) = \left\langle \Phi_E^i(R) \middle| \sqrt{\frac{\Gamma_i(R)}{2\pi}} \middle| \chi_{v0}(R) \right\rangle_R. \tag{14}$$

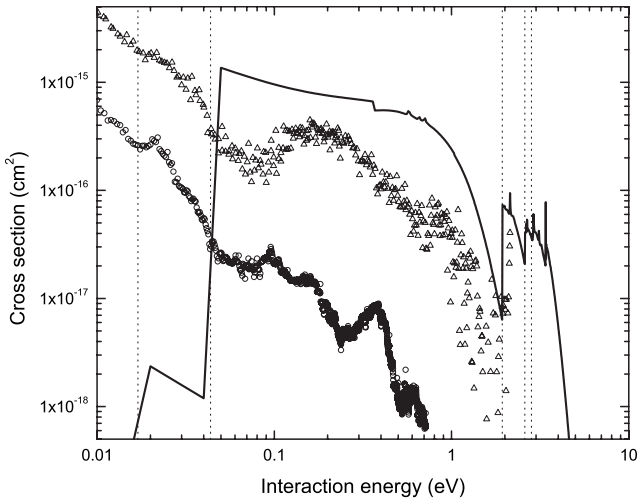

FIG. 8. Calculated total cross section using the local time-independent method. The experimental cross sections for DR and ion-pair formation measured at CRYRING are included for comparison [12]. The vertical lines correspond to the energies where the different asymptotic limits open up.

Here Φ_E^i is the continuum radial eigenstate with an energy of E for electronic state i. This matrix element is related to the electron capture probability into the resonant state i [29].

B. Total cross section

In Fig. 8, we show the calculated total cross section obtained by summarizing the cross sections from all 30 resonant states included in the calculation. We have used the local approximation for treating autoionization for all resonant states except for the $2\,^1\Sigma^+$ state where the nonlocal approximation has been applied. We also present in the same figure the measured cross sections for DR and ion-pair formation.

Since the electronic couplings between the neutral states are not included, the final state distributions cannot be determined and hence the total cross section that is given by the sum of the total DR and ion-pair cross sections is obtained. The calculated cross sections shows a sharp threshold at $E=0.04$ eV, where the $H(n=2)+F(^2P)$ channel becomes energetically open. Below this threshold, we obtain a cross section much smaller than the experimental cross section. Above this threshold, we overestimate the measured cross section a factor ranging from 6 (at 0.07 eV) to 1.5 (around 2 eV). Furthermore, we do not see the pronounced peak observed around 0.2 eV in the measured cross section. At 1.9 eV, there are peaks in the calculated cross section, where the higher resonant states become open for dissociation. This will be discussed below.

C. Threshold effects in the cross section

Thresholds occur when new resonant states become energetically open for dissociation. The threshold energies are indicated with vertical lines in Fig. 8 and also given in Table I. The $1\,^3\Sigma^+$ is the only resonant state that is energetically open for dissociation below 0.017 eV, where $1\,^1\Sigma^+$ become open, that is the ion-pair limit. Since the calculated cross section for these states are much lower than the other states in the model, we can conclude that below the threshold for the third resonant state ($E=0.04$ eV), the approximations applied in the present treatment break down. We do not in this calculation include the Rydberg states and the electronic couplings between the resonant states and the Rydberg manifold. The measured cross section below 0.04 eV could be explained by the indirect process, i.e., induced by nonadiabatic couplings the electron is first captured into a bound Rydberg state. This state is then predissociated through the electronic couplings to one of the resonant states that is open for dissociation. Another possible path to dissociation could be the capture of the electron into one of the higher resonant states that has a good Franck-Condon overlap with the vibrational wave function of the ion. This resonant state is not open for dissociation at low energies. The system remains in this state, and then couples to one of the Rydberg states, making one or several oscillations in this bound Rydberg state before being predissociated by the lowest resonant states. Our *ab initio* calculated adiabatic potentials show strong evidence of avoided crossings between the Rydberg states and the resonant states at small internuclear distances. We therefore believe there will be relative strong couplings between these states. For example, the ion-pair state $1\,^1\Sigma^+$ crosses the lowest Rydberg state of the same symmetry very close to its minimum and we have indications of strong couplings between these states. The experimentally observed $1/E$ dependence of the cross section at lower energies is normally characteristic for the direct process [35]. This might indicate that the second mechanism for the reaction is the path to dissociation at low collision energies.

The molecular ions in the ion-storage ring experiment are vibrationally cool, but not rotationally [12]. Therefore any threshold effects in the experiment will be smeared out by the rotational distribution. In the experimental cross section in Fig. 8 indications of new open channels can be seen. The most clearly visible threshold effect in the experimental DR cross section is where the "intermediate" resonant states open up for dissociation at 1.93 eV. At this energy our resonant states associated with the limit $H(n=3)+F(^2P)$ becomes open for dissociation. The threshold for the "higher" resonant states occurs at energies higher than what has been measured experimentally in CRYRING.

D. Contribution from lowest resonant states

The contributions to the cross section from the "lowest" resonant states [that is, all eight states dissociating into the three lowest asymptotic limits, i.e., H+F with H in $n=1,2$ and F in its ground state (^2P), as well as the ion-pair limit H^++F^-] together with the measured data of DR and ion-pair formation are presented in Fig. 9.

As discussed earlier, the two lowest states are the lowest $1\,^3\Sigma^+$ state and the ion-pair state $1\,^1\Sigma^+$. They both cross the ionic ground state potential at internuclear distances smaller than the equilibrium distance of HF^+. The cross sections for these two lowest resonant states are orders of magnitude

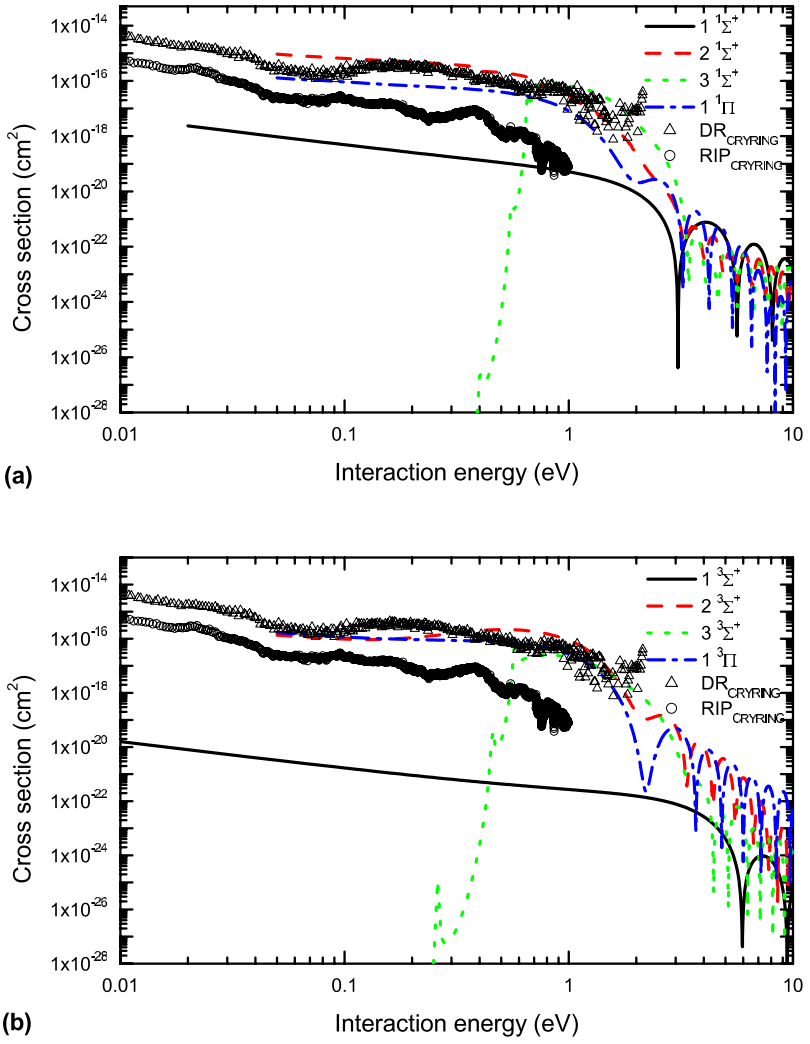

FIG. 9. (Color online) Contributions from the lowest resonant states to the cross section. Included in the figure are also the experimental cross sections for DR and ion-pair formation. (a) Contributions from singlet states. (b) Contributions from triplet states.

lower than the cross sections for the other resonant states as well as the experimental DR cross section. This can partly be understood by the negligible Franck-Condon overlap between the vibrational wave function of the $v=0$ of the ion and the continuum radial wave function of the resonant state. In the literature, there has been a debate as to whether or not the ion-pair state crosses the ground state of the HF^+ [12,14,15]. The present study supports the fact the diabatic ion-pair state indeed crosses the ionic potential, but it crosses the inner wall of the potential at a small internuclear distance ($R_x=1.3a_0$). Furthermore, the calculated direct dissociation into the ion pair underestimates the measured cross section for formation of $H^+ + F^-$ with a factor ranging from 100 (at 0.02 eV) to 1.5 (at 1 eV). Also the observed structure in the measured cross section is not seen in the calculated cross section.

Six electronic states ($2,3\ ^{1,3}\Sigma^+$ and $1\ ^{1,3}\Pi$) cross the ion potential close to its minimum. These electronic states are the main contributors to the total cross section in the energy region $0.04\ \text{eV} \leqslant E \leqslant 1.93\ \text{eV}$. The $3\ ^{1,3}\Sigma^+$ resonant states show an onset in the cross sections around 0.2–0.3 eV. This can be undestood by the barrier in the potential curves at these energies.

The calculated cross section from the lowest resonant states show a relative smooth energy dependence at collision energies below 1 eV. When they add up to the total cross section, total cross section is overestimated and we do not reproduce the observed structure in the measured cross section. It remains to be investigated if, e.g., interference effects induced by couplings between the electronic states may explain some of the observed structures.

E. Contribution from intermediate resonant states

In Fig. 10 we show the cross sections from the "intermediate states" that are associated with $H(n=4)$ and F in its ground state. These states have a threshold of 1.93 eV (see Table I). We also show the experimental DR cross section. The DR cross section was measured for collision energies up to 2 eV. At the threshold of the intermediate resonant states, the experimental cross section increases by almost a factor of 10.

The states that contribute most to the cross section in this region are the $5\ ^1\Sigma^+$, $5\ ^3\Sigma^+$, and $6\ ^1\Sigma^+$ states. The thresholds from these states coincide perfectly with experimental data.

The cross section for some of the states have strong sharp oscillations above threshold. These oscillations are physical in nature. The potential energy curves of the electronic states that show these resonant structures have barriers toward dissociation. The resonances above the dissociation limit are

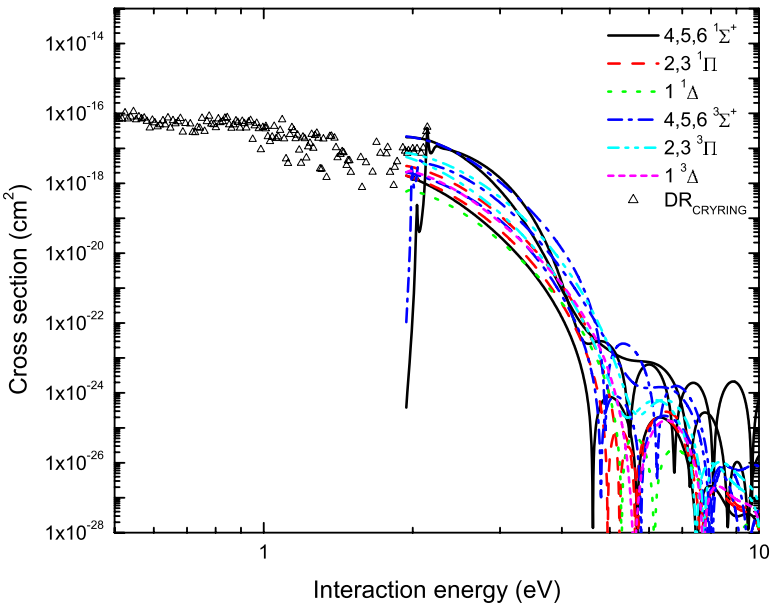

FIG. 10. (Color online) Contributions from the intermediate resonant states to the total cross section. Included is also the experimental cross section for DR.

thus shape resonances occurring at the energies where there is a large probability for tunneling through the barrier. Similar resonances have previously been seen in a theoretical study of DR of HeH^+ at low collision energies [36].

F. Contribution from highest resonant states

Contribution from the highest resonant states to the cross section are shown in Fig. 11. In this energy region, the total DR cross section is not measured. The states that contribute most strongly to the total cross section are the 7 $^1\Sigma^+$, 8 $^1\Sigma^+$, and 8 $^3\Sigma^+$ states.

We see sharp thresholds when the dissociation limits of these high-energy resonances open up. Note that if electronic couplings are included, these threshold effects may be smeared out.

V. CONCLUSIONS

We have calculated the resonant states relevant in electron recombination with HF^+. The resonant states are calculated by combining electron scattering calculations with MRCI structure calculations. The resonant states are Rydberg states converging to the excited states of the ion. By following the CI configurations of these excited ionic cores, the resonant states can be diabatized relative to the Rydberg manifold and the ionization continuum. The nuclear dynamics is described using both a time-dependent wave-packet technique as well as a time-independent approach, where a driven Schrödinger equation is solved. Autoionization from the resonant states is included using both a local and a nonlocal approximation. No electronic couplings between the neutral states are included in the present model. We found that 30 resonant states contribute to the cross section below 10 eV. The local ap-

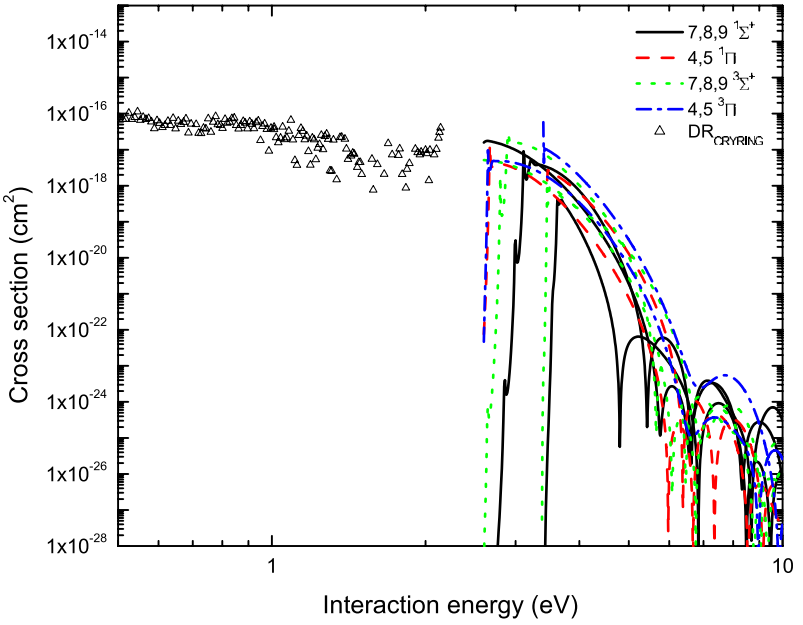

FIG. 11. (Color online) Contributions from the highest resonant states to the total cross section. Included is also the experimental cross section for DR.

proximation for treating autoionization is justified for the present system. We obtain a qualitative agreement with measured cross section from CRYRING [12], even though the calculated cross section is slightly larger and shows a smoother energy dependence. In agreement with our calculated cross section, the experimental cross section shows a clear threshold at $E=1.94$ eV, where the "intermediate" resonant states become open for dissociation.

We are not able to reproduce the cross section below 0.04 eV. We believe that we here need to include the electronic couplings in the theoretical model. This will couple resonant states that are energetically close for dissociation via the bound Rydberg states to resonant states that are open for dissociation. For a future study, we are calculating the relevant electronic couplings. The difficulty is that we here have an infinite number of Rydberg states interacting with the manifold of resonant states. The electronic couplings have to be calculated for all symmetries.

The cross section for direct dissociation along the $1\,^1\Sigma^+$ state that correlates with the ion-pair limit $H^+ + F^-$ is significantly smaller than the measured ion-pair cross section. In order to describe the ion-pair formation in electron recombination with HF^+, we will have to study the dynamics on the coupled states. We might also have to include the indirect capture into the Rydberg states that then are predissociated by the ion-pair state. It should be noted that the ion-pair state will couple to the Rydberg states only at small internuclear distances. Since the ion-pair state and the $H(n=2)+F$ limits are almost degenerate these states come close in energy for large internuclear distance and the electronic couplings between these states can there be neglected. We therefore believe that we will not obtain the clear interference structure seen in ion-pair formation in electron recombination with HD^+ [27]. Also in the experimental ion-pair cross section [12] there are no clear signs of such quantum interference between competing dissociative pathways.

ACKNOWLEDGMENTS

Å.L. acknowledges support from The Swedish Research Council and A.E.O. acknowledges support from the National Science Foundation, Grant No. PHY-05-55401.

[1] T. Hosino and Y. Nishioka, J. Chem. Phys. **111**, 2109 (1999).
[2] D. A. Neufeld, J. Zmuidzinas, P. Schilke, and T. G. Phillips, Astrophys. J. Lett. **488**, L141 (1997).
[3] See http://books.nap.edu/readingroom/books/planet_sci/contents/chap4b.html.
[4] M. Bettendorff, R. J. Buenker, S. D. Peyerimhoff, and J. Römelt, Z. Phys. A **304**, 125 (1982).
[5] P. Piecuch, A. E. Kondo, V. Špirko, and J. Paldus, J. Chem. Phys. **104**, 4699 (1996).
[6] E. Pahl, H.-D. Meyer, L. S. Cederbaum, and F. Tarantelli, J. Electron Spectrosc. Relat. Phenom. **93**, 17 (1998).
[7] D. Feller and K. A. Peterson, J. Mol. Struct.: THEOCHEM **400**, 69 (1997).
[8] R. K. Chaudhuri, K. F. Freed, S. A. Abrash, and D. M. Potts, J. Mol. Struct.: THEOCHEM **547**, 83 (2001).
[9] A. Brown and G. G. Balint-Kurti, J. Chem. Phys. **113**, 1870 (2000).
[10] D. R. Bates, Phys. Rev. **78**, 492 (1950).
[11] J. N. Bardsley, J. Phys. B **1**, 365 (1968).
[12] N. Djurić, G. H. Dunn, A. Al-Khalili, A. M. Derkatch, A. Neau, S. Rosén, W. Shi, L. Vikor, W. Zong, M. Larsson, A. Le Padellec, H. Danared, and M. af Ugglas, Phys. Rev. A **64**, 022713 (2001).
[13] A. J. Yencha, A. Hopkirk, J. R. Grover, B.-M. Cheng, H. Lefebvre-Brion, and F. Keller, J. Chem. Phys. **103**, 2882 (1995).
[14] Q. J. Hu and J. W. Hepburn, J. Chem. Phys. **124**, 074311 (2006).
[15] Q. J. Hu and J. W. Hepburn, J. Phys.: Conf. Ser. **4**, 267 (2005).
[16] T. N. Rescigno, B. H. Lengsfield, and C. W. McCurdy, in *Modern Electronic Structure Theory* edited by D. R. Yarkony (World Scientific, Singapore, 1995), Vol. 1, p. 501.
[17] S. Geltman, *Topics in Atomic Collision Theory* (Academic Press, New York, 1997) p. 31.
[18] D. G. Truhlar, J. Comput. Phys. **10**, 123 (1972).
[19] J. E. Sansonetti, W. C. Martin, and S. L. Young, *Handbook of Basic Atomic Spectroscopic Data* (NIST, Gaithersburg, MD, 2005); see http://physics.nist.gov/PhysRefData/Handbook/index.html.
[20] G. Herzberg, *Molecular Spectra and Molecular Structure: Vol 1, Spectra of Diatomic Molecules*, 2nd ed. (Van Nostrand Reinhold, New York, 1950).
[21] F. N. Fritsch and R. E. Carlson, J. Chem. Phys. **93**, 570 (1980).
[22] A. Goldberg, H. M. Schey, and J. L. Schwartz, Am. J. Phys. **35**, 177 (1967).
[23] C. W. McCurdy and J. L Turner, J. Chem. Phys. **78**, 6773 (1983).
[24] A. E. Orel, Phys. Rev. A **62**, 020701(R) (2000).
[25] C. S. Trevisan, K. Houfek, Z. Zhang, A. E. Orel, C. W. McCurdy, and T. N. Rescigno, Phys. Rev. A **71**, 052714 (2005).
[26] U. V. Riss and H. D. Meyer, J. Chem. Phys. **105**, 1409 (1996).
[27] Å. Larson and A. E. Orel, Phys. Rev. A **64**, 062701 (2001).
[28] K. C. Kulander and E. J. Heller, J. Chem. Phys. **69**, 2439 (1978).
[29] T. F. O'Malley, Phys. Rev. **150**, 14 (1966).
[30] T. N. Rescigno and C. W. McCurdy, Phys. Rev. A **62**, 032706 (2000).
[31] C. W. McCurdy, M. Baertschy, and T. N. Rescigno, J. Phys. B **37**, R137 (2004).
[32] B. Simon, Phys. Lett. **71A**, 211 (1979).
[33] P. Hislop and I. M. Sigal, *Shape Resonances in Quantum Mechanics*, Proceedings of the International Conference on Differential Equations and Mathematical Physics, 1986, edited by I. W. Knowles and Y. Saito, Lect. Notes in Math. (Springer-Verlag, Birmingham, Albama, 1987), 1285.
[34] O. Motapon, M. Fifirig, A. Florescu, F. O. Waffeu Tamo, O. Crumeyrolle, G. Varin-Bréant, A. Bultel, P. Vervisch, J. Tennyson, and I. F. Schneider, Plasma Sources Sci. Technol. **15**, 23 (2006).
[35] E. P. Wigner, Phys. Rev. **73**, 1002 (1948).
[36] Å. Larson and A. E. Orel, Phys. Rev. A **72**, 032701 (2005).